Purdue University
Purdue e-Pubs

International Refrigeration and Air Conditioning Conference

School of Mechanical Engineering

2018

Vapor Compression Refrigeration System for Cold Storage on Spacecrafts

Cai Stephen Rohleder
Purdue University, crohlede@purdue.edu

Kunal Bansal
Air Squared Inc, CO United States of America, k.bansal@airsquared.com

Bryce Shaffer
Air Squared Inc, CO United States of America, bryce@airsquared.com

Eckhard A. Groll
Purdue University - Main Campus, groll@purdue.edu

Follow this and additional works at: https://docs.lib.purdue.edu/iracc

Vapor Compression Refrigeration System for Cold Storage on Spacecrafts

Cai S. ROHLEDER[1]*, Kunal BANSAL[2], Bryce SHAFFER[2] and Eckhard A. GROLL[1]

[1] Ray W. Herrick Laboratories, Purdue University
177 S Russell Street, West Lafayette, IN, 47907-2099, USA
crohlede@purdue.edu, groll@purdue.edu

[2]Air Squared Inc.,
510 Burbank Street, Broomfield, CO, 80020, USA
k.bansal@airsquared.com, bryce@airsquared.com

* Corresponding Author

ABSTRACT

NASA's future missions include sending astronauts back to the moon, and further. Challenges associated with these goals are not limited to the science involved with propelling these astronauts to their destination. In fact, life support systems must also advance to improve astronaut health during their long flights in space. Currently, food consumed in space is processed to be shelf stable, and recent experiments have shown that nutrients of these shelf stable foods decay over time (Cooper, Perchonok, & Douglas, 2017). Refrigeration storage for more nutritional food has remained undeveloped due to fluid flow and heat transfer management difficulties in microgravity. As part of a NASA SBIR Phase I project, the project team has designed a modular refrigerator that is able to preserve food in a frozen state. The proposed vapor compression cycle (VCC) reduces the instability of flow in microgravity through both reduction on liquid reliance via a coupled oil-free scroll compressor and expander, and through specific methods of design that manage two-phase refrigerant flow through the heat exchangers. R134a is the working fluid, as it is non-toxic, non-flammable, has favorable volumetric characteristics, and will be available in the future. Air is pulled across the evaporator of the vapor compression loop to be cooled, and then fed into four identical food storage compartments. Absorbed heat from the air is rejected out of the condenser into a central cooling water loop in the spacecraft. Developments of more effective vapor compression systems in space may also yield improved systems for use on earth.

1. INTRODUCTION

Astronauts eat shelf stable food while in space, although these foods lose their nutritional stability over time during storage (Cooper, Perchonok, & Douglas, 2017). To improve the quality and maintain appropriate nutritional content of the food eaten in space, use of a vapor compression refrigeration heat pump similar to terrestrial systems is proposed as part of a NASA SBIR Phase 1 project awarded to the project team. The main components of the proposed heat pump consist of a four-chamber refrigerated space, an oil-free scroll compressor and expander, a fin and tube evaporator, and a co-axial tube-in-tube condenser. The effects of microgravity in space were accounted for in the design of each component.

Previous research on heat pumps in space has been mostly limited to their feasibility and has discussed the various challenges associated with microgravity. The Vought Systems Division at LTV Aerospace (1974) conveyed that a vapor compression system is the preferred method for refrigeration in space. Hye (1983) designed a vapor compression refrigeration system for Spacelab, and determined that large Froude and Reynolds numbers would be necessary to establish high heat transfer coefficients in the heat exchangers, as well as to maintain appropriate fluid flow rate and pattern throughout the system. Hye (1985) also considered the hazardous effect of leakages in his design, as many refrigerants are harmful when in contact with humans. The proposed system used a diaphragm compressor to isolate lubricants from the refrigerant loop, and double containment to reduce risk of exposure in the event of a refrigerant leak. To limit the need for oil management, Cole *et al.* (2006) proposed the design of a heat pump that used a rotary screw compressor, which required little oil to lubricate its bearings, and also used single-circuit, counter-flow, tube-in-tube heat exchangers, which were optimized for stability and gravity independence.

Furthermore, Ruemmele *et al.* (2006) recommended the use of a refrigerant that was safe to use in a closed crew environment.

The proposed design considered here takes these past projects into account and eliminates certain concerns by simplifying the design. In particular, there is no need for fluid separation between lubricant and refrigerant as the compressor and expander are oil-free technologies with permanently sealed greased bearings that are not exposed to the refrigerant loop. R134a was chosen to be the working fluid as it is not flammable, hazardous to humans, and had favorable performance characteristics. The condenser and evaporator were designed such that annular flow is maintained throughout the heat exchange process in both heat exchangers.

In this paper analytical and iterative methods are used to size and optimize the components of the system, while a parametric study is performed to select the best working fluid. Additionally, two compressors are tested to determine performance at the design operating conditions.

2. SYSTEM REQUIREMENTS

NASA provided design targets that bound the design space of the refrigeration system. The overall objective is long term storage of large amounts of food in a cooled space that can be accessed weekly or biweekly. In this way, the heat capacity requirements of the system are minimized by reducing the frequency of accessing the refrigerated space. The refrigerated space was selected to be $2 \, m^3$, with a food density of $480 \frac{kg}{m^3}$, and a maximum air temperature of $-22 \, °C$. The spacecraft's main chilled water loop is used for heat rejection with a water inlet temperature of $20 \, °C$. The entire unit is exposed to cabin conditions of air at $23 \, °C$ and 1 atm. The food will be pre-frozen, negating product heat loads. The unit must be able to withstand launch forces (up to 7 g's), using materials with a secondary mass penalty below $0.2 \, kg$ per kg of food. Additionally, the unit must not draw more than $0.15 \, W$ per kg of food. Due to organizational and spatial concerns, the refrigerated space is divided into four equal compartments, each with their own access door. To reduce the equipment load of the cooled space, the vapor compression components are in a separate space, located at the top of the unit.

2.1 Heat Load

After material selection and geometrical constraints established, the heat load entering the refrigerated space is calculated by considering four different contributions: (i) transmission heat load due to heat transfer from the environment; (ii) internal heat load generated from electrical equipment inside the cooled space; (iii) infiltration heat load due to access of the space from the outside; (iv) equipment load generated from the vapor compression equipment itself. Equipment load is neglected as the components are separated from the space, the components are properly insulated, and the compressor is hermetic so that heat is only applied to the refrigerant. As some of this load is determined from equipment selection after design of a refrigeration system, the load calculations were an iterative process.

The internal heat load was determined after volumetric flow requirements were calculated, where the evaporator fan is assumed to be the major contributing factor. After averaging the energy requirements for several commercially available fans, a factor of safety of 1.2 was selected to make up the internal heat load.

Air infiltration loads were calculated based on ASHRAE recommendations and equations on the subject (ASHRAE 2002). It was assumed that the refrigerated space would be accessed once per week, time to open or close the door takes 3 seconds, and during access the door would be open no longer than 1 minute. The equations used were based on those times, as well as the properties of the air infiltrating the refrigerated space, and the air already in the refrigerated space. Some equations used also include effects of gravity. The assumption made is that these equations are applicable in a microgravity environment, although instead of using earth's gravity, a coefficient of $1 \frac{m}{s^2}$ was used so as not to amplify or mitigate the effects of gravity. With these assumptions, the infiltration heat load was calculated, by also including a factor of safety equal to 1.2.

Transmission load is the predominant heat load on the system. The air temperature difference between the cabin air and the refrigerated air is at least $45 \, °C$. Due to this large temperature difference, heat transfer through the walls will have to be determined. The walls were designed to ensure structural integrity during launch. In particular, the walls surrounding the refrigerated space are composed by two layers of titanium separated by vacuum panels. Convection

from air to walls, radiation across the vacuum panel, and conduction through the walls is considered. Heat transfer coefficients (HTC's) were calculated for both convection and radiation, while thermal conductivity constants were used for conduction through the walls. Figure 1 shows a schematic of the thermal circuit used in calculating the transmission loads.
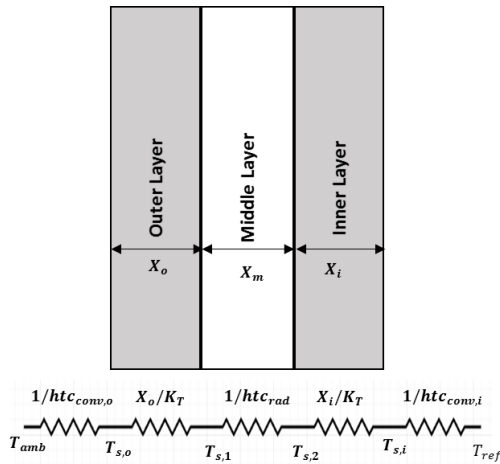

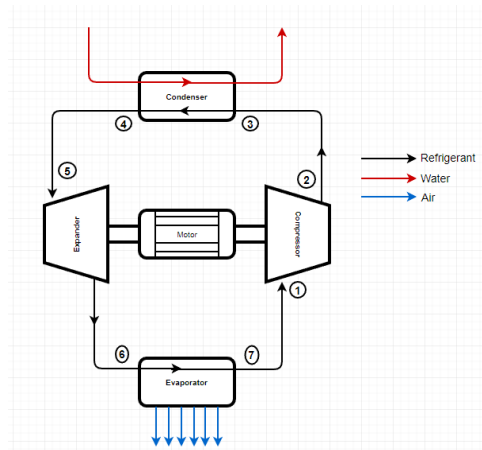**Figure 1:** Thermal circuit of the system walls.

Figure 2: VCC cycle in the proposed cold food storage system. Note that air rejects heat into the evaporator, and water absorbs heat from the condenser.

It is assumed that there is low air velocity on both sides of the wall. A correlation for flow over a flat plate from Incropera et al. (2006) is used to determine the convective HTC's, while a different correlation for radiative heat transfer between two infinite parallel plates is used from the same source to calculate the radiative HTC. The thermal heat transfer across the structure of the vacuum panels themselves is neglected. The main equations used to determine the transmission heat load are reported in Equations (1) to (5). Note that a 1.2 factor of safety was implemented in Equation (5).

$$Nu = 0.664 * (Re)^{\frac{1}{2}} * (Pr)^{\frac{1}{3}} \tag{1}$$

$$htc_{conv} = \frac{Nu * k_{air}}{l} \tag{2}$$

$$htc_{rad} = \frac{\left(\sigma * (T_{s_1} - T_{s_2}) * \left((T_{s_1})^2 - (T_{s_2})^2 \right) \right)}{\left(\frac{1}{\varepsilon m_{s_1}} \right) - \left(\frac{1}{\varepsilon m_{s_2}} \right) - 1} \tag{3}$$

$$U_{Overall} = \frac{1}{\left(\frac{1}{htc_{conv_o}} \right) + \left(\frac{X_o}{k_T} \right) + \left(\frac{1}{htc_{rad}} \right) + \left(\frac{X_i}{k_T} \right) + \left(\frac{1}{htc_{conv_i}} \right)} \tag{4}$$

$$\dot{Q} = 1.2 * U * A_{s_{ref}} * (T_{amb} - T_{ref\ space}) \tag{5}$$

The calculated heat loads found are listed in Table 1. To be noted is that the transmission load is significantly larger than the other considered loads. With a total load of $168\ W$, only a small capacity VCC will be necessary to condition the refrigerated space.

Table 1: Heat loads applied to the refrigerated space.

Parameter	Heat Load [W]
Transmission Load	142.5
Internal Load	24
Infiltration Load	1.73
Total Load	168.2

2.2 Selection of Refrigerant
In order to determine the best refrigerant for use in the vapor compression cycle (VCC), a simple thermodynamic model of the cycle was developed by using Engineering Equation Solver (EES) (F-Chart Software, 2017). The

model included the four main components in the cycle, i.e., the compressor, condenser, expander, and evaporator. The driving value of the model was the necessary evaporator capacity calculated previously. Initial assumptions about superheating, subcooling, compressor efficiency, expander efficiency, and motor efficiency were made. Known operating conditions were the evaporating and condensing temperatures and the temperature difference across both heat exchangers. The schematic of the system detailing the connections between each component can be seen in Figure 2. A parametric study was conducted to evaluate the performance of the system for different working fluids. Each refrigerant was investigated and compared primarily based on the following requirements:

1. Thermodynamic performance
2. Future availability
3. Volumetric characteristics across the compressor
4. Safety

Given the operating conditions, the model determined specific enthalpy, specific volume, and specific entropy of the refrigerant at each state point, as well as the mass flow rate of refrigerant flowing through the cycle. Using both mass flow rate and the specific enthalpy across the compressor, the input work necessary for the cycle to operate was calculated. This input work is reduced by the work recovered by the expander, and then compared to the evaporator capacity to determine the COP of the cycle, which is expressed by:

$$COP = \frac{\dot{Q}_{Evap}}{\dot{W}_{Comp} - \dot{W}_{Expand}} \tag{6}$$

Four refrigerants, i.e. HFC R134a, HFO R1234yf, and the natural refrigerants Isobutane and Isopentane, were the best performers. As the natural refrigerants are flammable, and R1234yf is mildly flammable and performed thermodynamically worse than R134a, R134a was ultimately chosen as the working fluid in the refrigeration system.

3. COMPONENT DESIGN

Each component was designed based on the specifications obtained from the thermodynamic model. As the system is intended for use in microgravity, the designs were tailored to ensure ideal flow characteristics in a microgravity environment. Microgravity particularly influenced the design of the evaporator and condenser.

3.1 Evaporator Design
The storage unit will be maintained cool by means of a fin and tube evaporator that absorbs heat from the air inside the unit. The geometry of the unit was determined via the following iterative design process:

1. Pre-establish evaporator geometry
2. Set the number of rows deep and rows high of refrigerant tubing, and the fin pitch
3. Determine heat capacity of evaporator at design conditions
4. Compare heat capacity to the required heat capacity of the simple model
5. Adjust number of rows and columns of refrigerant tubing, and fin pitch accordingly
6. Repeat steps 3 through 5 until evaporator model matches heat capacity design requirements

Due to the fact that fluid flow management becomes increasingly difficult in microgravity, the evaporator design has only one inlet and one outlet. This means that the entire refrigerant will flow through all of the coils, and will not be divided into multiple circuits. The diameter of the refrigerant tubing in the evaporator coils was designed to be 5 mm in diameter regardless of other dimensional changes, as the flow pattern of the refrigerant is determined primarily by the refrigerant tubing diameter. It is important to maintain an annular flow pattern as annular flow yield the highest two-phase heat transfer rate. Flow pattern predictions were based on flow maps specific to flow in microgravity created by Jayawardena et al. (1997). These maps relate superficial Reynolds numbers and the Suratman number. Based on the maps, the required mass flowrate, and the refrigerant properties as R134a flows through the evaporator, annular flow is predicted to occur throughout the evaporator until full vaporization, with decreasing liquid film thickness as refrigerant quality increases.

With an established tubing diameter that yields annular flow, heat transfer correlations for annular flow from Liu and Winterton (1991) were used to predict the heat transfer coefficient of the refrigerant. This correlation relates the

two phase heat transfer coefficients to convective heat transfer and nucleate boiling heat transfer, and both terms are multiplied by a coefficient determined by the fluid properties and the Reynolds and Prandtl numbers.

The heat transfer coefficients of the air flowing over the coils are determined using a correlation from Wang et al. (2000). This correlation determines heat transfer of each row relative to the other rows via the Coburn factor, which is related to the Nusselt number. The heat capacity of the evaporator was predicted using the NTU-effectiveness method. An overall heat transfer coefficient of the evaporator was calculated from the heat transfer coefficient of the refrigerant inside the coils and the heat transfer coefficient of the air passing over the coils in combination with their respective flow areas. In the iterative process, the numbers of rows and columns as well as the fin pitch were the main determinants of the evaporator heat capacity. The geometry of the evaporator is illustrated in Figures 3 and 4.
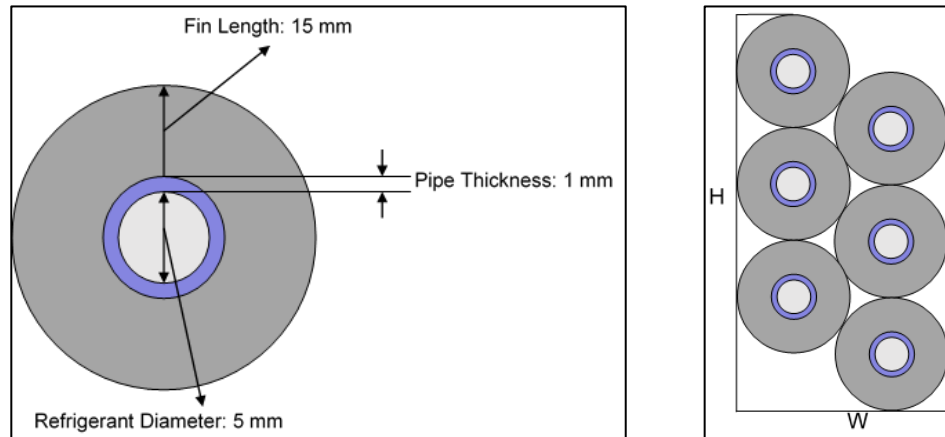

Figure 3: Cross section of the refrigerant tubing. On the left, a single tube is shown, displaying the thicknesses of the pipe and fin. On the right, an example evaporator which is 2 rows deep and 3 rows high. The evaporator is in a staggered orientation. Note that the final design is 12 rows deep and 6 rows high.
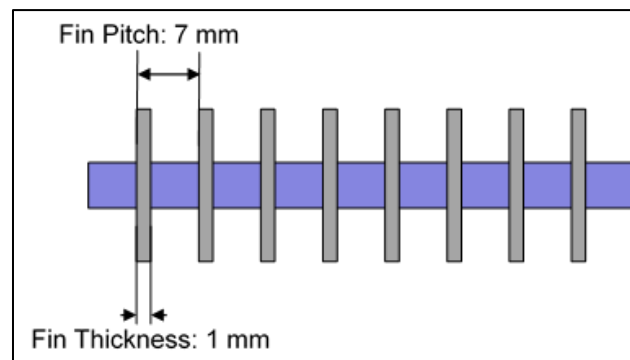

Figure 4: Alternative cross section with fin pitch displayed. A wide fin pitch was used to reduce air pressure drop across the coils as ice buildup occurred.

3.2 Condenser Design

Water from a chilled water loop inside the spacecraft is supplied to the storage unit to provide a medium for heat rejection from the condenser. A concentric tube in tube condenser with twisted tape inserts was designed to reject heat to the cooling water. Water flows in the annulus of the condenser tubing, while the refrigerant flows in the center tubing. Condensing fluids in microgravity have reduced flow stability (LTV Aerospace, Vought Systems Division, 1974). Therefore, twisted tape inserts are used to increase flow stability by passively forcing annular flow of the refrigerant through radial directional changes of the refrigerant flow path inside the center tube. This additional material inside the refrigerant tube also enhances heat transfer from the refrigerant by increasing surface area. Similar to the evaporator design, there is only one circuit/flow path for the refrigerant to follow in the condenser, which simplifies design and increases control over the refrigerant flow. The geometry of the condenser is illustrated in Figure 5.
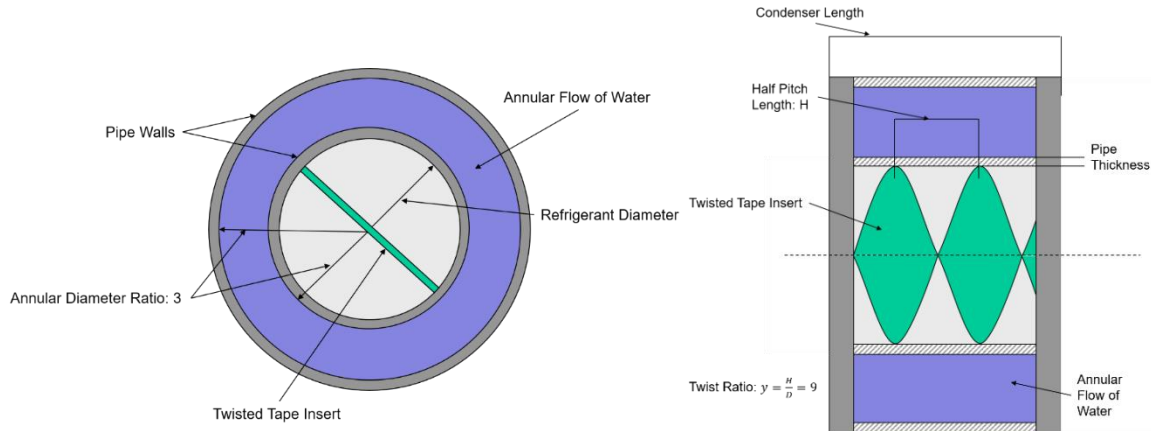
Figure 5: Condenser geometry. On the left is a cross section of the condenser displaying the annular flow of the water around the refrigerant tubing. On the right is a half section view of the design displaying the twisted tape inside the refrigerant piping. Blue indicates water flow while light grey indicates refrigerant flow.

Similar to the evaporator, portions of the condenser geometry are predefined before analysis. There are less variables in the geometry of the condenser however, which removes the need for iteration, and leads to the correct condenser dimensions solely through analytical methods. The condenser was designed by fixing all dimensions/ geometries except for the total length of the condenser, which was calculated based upon the necessary condenser heat capacity predicted by the model. Larger heat capacity requirements lead to a longer condenser, whereas lower heat capacity leads to a reduced condenser length. As the refrigerant flows in three different phases inside the condenser (superheated vapor, two-phase, and subcooled liquid), the moving boundary method is employed to predict the heat capacity. Each fluid phase has a local NTU-effectiveness method applied, with boundaries determined by balancing the heat transfer rate of the refrigerant with that of the water. To determine the overall heat transfer coefficient in each boundary, correlations were used to find the heat transfer coefficient of the refrigerant and the water. A correlation for flow of R134a including twisted tape inserts by Akhavan-Behabadi et al. (2008) is used. This correlation uses an adjusted Reynolds number which is dependent on the twist ratio of the twisted tape. For the water in the annulus, a correlation by Dirker and Meyer (2005) is used.

A 3D CAD software was used to render the heat exchanger designs, as well as the initial storage unit concept. The evaporator and condenser are depicted in Figure 6. Figure 7 presents a partial rendering of the first prototype storage unit, which excludes the structural and modular capabilities of the actual design.
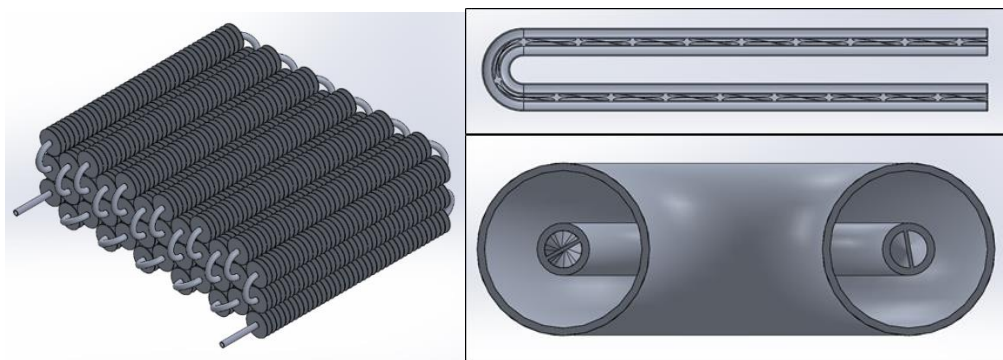

Figure 6: 3D rendered designs of the evaporator (left) and the condenser (right). A cut view of the condenser (bottom right) displays the inner tubing of the refrigerant line, as well as the twisted tape inside the refrigerant tubing.
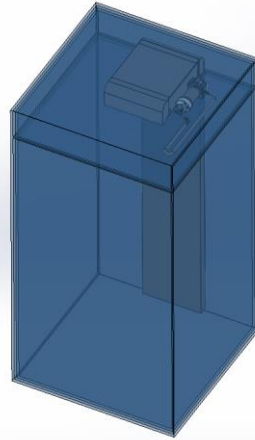
Figure 7: Partial Prototype design of the storage unit. The vapor compression system sits atop the refrigerated space. There is ducting from the bottom of the refrigerated space, around the evaporator, and back into the refrigerated space at the top.

4. COMPRESSOR TEST RESULTS

A modified off-the-shelf orbiting two-stage idler-shaft scroll pump was placed on a hot-gas bypass test stand. Three modifications were made to change the scroll pump into a scroll compressor before it was tested. In particular, the idler-shaft springs were replaced with hard shims, converting the "floating" two stage design to a "set tip gap" design, the bearing grease was changed to fluid grease, and the motor was changed to a higher power motor, which was connected to the scroll head externally via magnetic couplings. The test bench is shown in Figure 8.

A hot-gas bypass test stand allows the operator to quickly test a compressor at multiple operating conditions. The test stand does not use an evaporator, while ensuring that vapor enters the compressor by mixing superheated vapor with condensed refrigerant just before the compressor. This superheated vapor comes from a bypass loop out of the compressor, which is expanded and then sent back to the compressor inlet after mixing. The design operating conditions for the compressor are shown in Table 2.

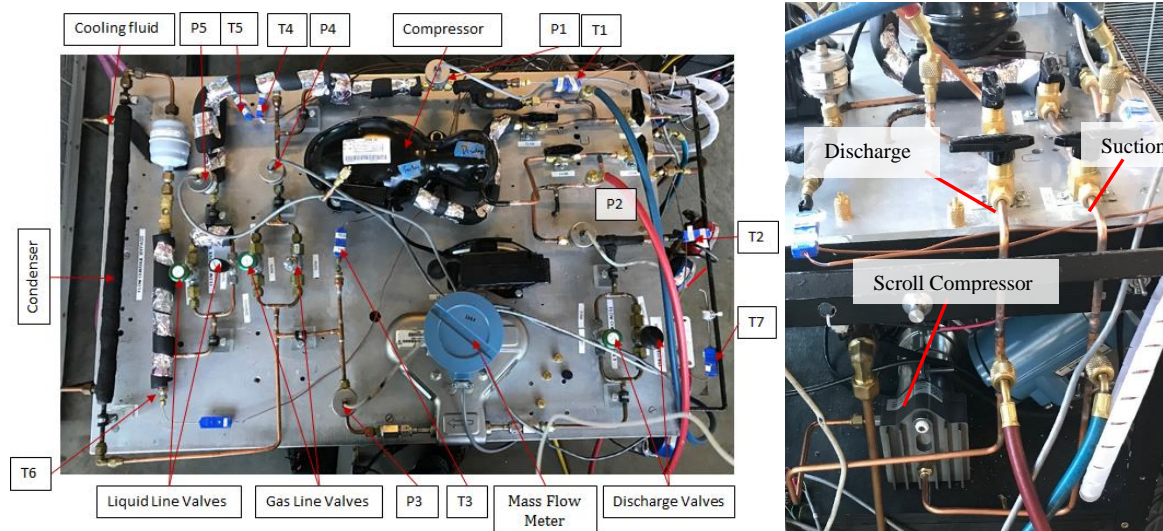**Figure 8:** Hot-gas bypass test stand used in testing the scroll compressor (right) and an alternative linear compressor (left). The original project considered only scroll compressor technology.

Compressor performance tests were conducted at various operating points. Unfortunately, the preliminary tests were limited due to two main issues: decoupling of the magnets that connected the scroll head shaft to the motor shaft,

and a low condenser capacity on the test bench which led to little or no subcooling on the condenser line. Despite these issues, some successful tests were performed and the results are listed in Table 3

Table 2: Design Operating conditions of the compressor.

$T_{Evaporator}$	-32 °C
$P_{Evaporator}$	11.13 psi (76.71 kPa)
$T_{Condenser}$	30 °C
$P_{Condenser}$	111.18 psi (770.6 kPa)
$T_{Superheat}$	5 °C
$\dot{m}$	1.141 g/s

Table 3: Operating conditions of the scroll compressor.

Test	Speed [RPM]	Evap. Temp. [C]	Cond. Temp [C]	Superheat [K]	Inlet Pressure [kPa]	Inlet Temp. [C]	Outlet Pressure [kPa]	Outlet Temp. [C]
1	1482	0.82	25.04	15.59	301.78	16.41	666.52	56.63
2	1561	-18.87	5.46	24.57	139.41	5.70	355.49	45.06
3	1564	-31.08	10.65	47.84	80.19	16.76	423.96	41.29
4	1755	-16.62	14.97	31.44	153.34	14.82	488.29	62.98
5	1969	-8.89	22.17	8.79	209.67	-0.10	611.50	79.47
6	2231	-9.07	22.75	10.74	208.22	1.67	622.25	81.67
7	2529	-8.65	22.50	8.37	211.67	-0.28	617.63	78.81

By utilizing the data collected at the given operating conditions and the refrigerant properties of R134a, performance ratings of the compressor can be calculated. The ratings are listed in Table 4. To be noted is that the test numbers correspond to the same test conditions reported in Table 3.

By analyzing the results, the performance of the compressor varied widely between the test conditions. High levels of work from the motor were necessary to achieve the relatively low rotational speeds, which can be attributed to the low compressor efficiencies, as well as the high superheat caused by the test stand. The vacuum pump selected for this initial testing was not optimized for the pressure ratios of the application. This leads to low compressor efficiencies, which increases the work and strain on the magnetic coupling and causes the magnets to decouple when higher rotational speeds were attempted. Due to the decoupling of the magnets between the shaft of the scroll head and the motor shaft at increasing work levels, the modified compressor was not able to achieve the design conditions of the storage unit. The closest test to the design operating conditions was Test 3. The evaporating temperature of the storage unit was achieved, but the condensing temperature was not achieved. This test had acceptable levels of volumetric and compressor efficiencies, but a low mechanical efficiency at 30%. An attempt to achieve the condensing temperature was made, but a steady state condition was never achieved due to magnetic decoupling.

Table 4: Scroll compressor performance data

Test	Pressure Ratio [−]	Differential Pressure [kPa]	Temp. Lift [K]	Mass Flowrate $\left[\frac{kg}{s}\right]$	Work Input [W]	Vol. Eff. [−]	Comp. Eff. [−]	Mech. Eff. [−]	Motor Eff. [−]
1	2.21	364.73	24.22	0.00248	244.2	0.88	0.37	0.70	0.79
2	2.55	216.08	24.33	0.00096	133.2	0.70	0.40	0.70	0.79
3	5.29	343.77	41.73	0.00046	198.9	0.61	0.66	0.30	0.79
4	3.18	334.95	31.59	0.00085	197.9	0.52	0.49	0.60	0.79
5	2.92	401.83	31.06	0.00159	323	0.58	0.48	0.53	0.79
6	2.99	414.03	31.82	0.00175	551.9	0.57	0.49	0.35	0.79
7	2.92	405.96	31.15	0.00210	478.3	0.59	0.48	0.45	0.79

It is predicted that with an optimized scroll compressor design, the design operating conditions can be met with greatly increased efficiencies. A similar sized oil free linear compressor was also tested at the design operating conditions of the storage unit. The results from this test are reported in Table 5.

The alternative compression technology of a linear compressor will be able to meet the needs of this project as well, providing a viable alternative to the scroll compressor. The efficiency of the compressor is high, even though a high superheat caused by the test stand lead to increased work input. In further phases of the project, both compressor designs will be considered.

Table 5: Linear Compressor Test at the design operating conditions of the storage unit.

Evap. Temp. [C]	Cond. Temp [C]	Superheat [K]	Inlet Pressure [kPa]	Inlet Temp. [C]	Outlet Pressure [kPa]	Outlet Temp. [C]	Mass Flowrate $[\frac{kg}{s}]$	Work Input [W]	Overall Eff. [%]
-31	30.3	44.69	80.26	13.69	776.35	55.42	0.00067	58.4	64.99

5. CONCLUSIONS AND FUTURE WORK

Preliminary design of a refrigerated food storage unit for use in space lead to components tailored specifically for the challenges found in a microgravity environment. This unit is based off a traditional four component vapor compression system often used in terrestrial refrigerator freezers.

While these components are theoretically predicted to work, the designs were based on correlations and therefore, manufacturing and testing of the heat exchangers must be performed to prove the design. The SBIR Phase II of this project has been approved, with testing of the entire system to occur, including the heat exchangers.

Ducting from the bottom of the refrigerated space, around the evaporator, and back into the top of the refrigerated space forces air circulation. The components are all located close to one another to minimize the size of the unit, reduce pressure drop across long lengths of pipe, and reduce the amount of refrigerant charge.

Design and manufacture of a new scroll compressor and expander, along with a linear compressor is also intended in Phase II. Each compressor will be tested in the cycle and compared.

NOMENCLATURE

A	Area	[m^2]
COP	Coefficient of Performance	[$-$]
ε	Effectiveness, Efficiency, Emissivity	[$-$]
g	Gravity	$[\frac{m}{s^2}]$
H	Height	[m]
h	Specific Enthalpy	$[\frac{kJ}{kg\,K}]$
htc	Heat Transfer Coefficient	$[\frac{W}{m^2\,K}]$
$\dot{m}$	Mass flowrate	$[\frac{kg}{s}]$
k, or K	Thermal Conductivity	$[\frac{W}{m\,K}]$
l	Length	[m]
Pr	Prandtl Number	[$-$]
$\dot{Q}$	Heat load	[W]
Re	Reynolds Number	[$-$]
ρ	Density	$[\frac{kg}{m^3}]$
σ	Boltzmann Constant	$[\frac{J}{K}]$

T	Temperature	$[C]$
U	Calculated Heat Transfer Coefficient	$\left[\frac{W}{m^2\,K}\right]$
$\dot{W}$	Work	$[W]$
X	Distance	$[m]$

Subscript

air	Air properties and contributions
amb	Ambient
Comp	Compressor
Cond	Condenser
conv	Convective/Convection
Evap	Evaporator
i	Inner
m	Middle
rad	Contributions from radiation
ref space	Refrigerated Space
s	Surface, Statepoint
T	Titanium properties

REFERENCES

Akhavan-Behabadi, M. A., Kumar, R., & Rajabi-najar, A. (2008). Augmentation of heat transfer by twisted tape inserts during condensation of R-134a inside a horizontal tube. *Heat and Mass Transfer*, 651-657.

ASHRAE. (2002). ASHRAE Handbook Chapter 12: Refrigeration Load.

Cole, G. S., Scaringe, R. P., Grzyll, L. R., & Ewert, M. K. (2006). *Development of a Gravity-Insensitive Heat Pump for Lunar Applications.* Houston: NASA.

Cooper, M., Perchonok, M., & Douglas, G. L. (2017). Initial Assesment of the Nutritional Quality of the Space Food System Over Three Years of Ambient Storage. *npj Microgravity*.

Dirker, J., & Meyer, J. P. (2005). Convective Heat Transfer Coefficients in Concentric Annuli. *Heat Transfer Engineering*, 38-44.

F-Chart Software. (2017). Engineering Equation Solver. Wisconsin. Retrieved from http://www.fchart.com/contact/

Hye, A. (1983). The Design and Development of a Vapor Compression Refrigerator/Freezer for Spacelab. *Thirteenth Intersociety Conference on Environmental Systems.* San Francisco: SAE.

Hye, A. (1985). Safety Considerations in the Design of Spacelab Refrigerator/Freezer. *Fifteenth Intersociety Conference on Environmental Systems.* San Fransisco: SAE.

Incropera, F. P., DeWitt, D. P., Bergman, T. L., & Lavine, A. S. (2006). *Fundamentals of Heat and Mass Transfer.* John Wiley & Sons.

Jayawardena, S. S., Balakotaiah, V., & Witte, L. C. (1997). Flow Pattern Transition Maps for Micgrogravity Two-Phase Flows. *AIChE Journal*, 1637-1640.

Liu, Z., & Winterton, R. H. (1991). A general correlation for saturated and subcooled flow boiling in tubes and annuli, based on a nucleate pool boiling equation. *Int. J. Heat Mass Transferq*, 2759-2766.

LTV Aerospace, Vought Systems Division. (1974). *Space Shuttle Orbiter Mechanical Refrigeration System.* Houston.

Ruemmele, W., Ungar, E., & Cornwell, J. (2006). *Vapor-Compression Heat Pumpsm for Operation Aboard Spacecraft.* Houston: NASA.

Wang, C.-C., Chi, K.-Y., & Chang, C.-J. (2000). Heat transfer and friction characteristics of plain fin and tube heat exchangers, part II: Correlation. *International Journal of Heat and Mass Transfer*, 2693-2700.

AKNOWLEDGEMENTS